SSRG International Journal of Civil Engineering
ISSN: 2348-8352/ https://doi.org/10.14445/23488352/IJCE-V13I6P112

Volume 13 Issue 6, 169-186, June 2026


*Original Article*

# Physics-Informed Neural Network Using LSTM Architecture for Transient Thermal Analysis of a Concrete Highway Bridge Deck

Berhanu Tefera[1], Adil Zekaria[2], Abrham Gebre[3]

[1,2,3]*Department of Civil and Environmental Engineering, College of Technology and Built Environment, Addis Ababa University, Addis Ababa, Ethiopia.*

[1]*Corresponding Author : berhanu.tefera@ddu.edu.et*

Received: 13 March 2026 Revised: 12 April 2026 Accepted: 11 May 2026 Published: 30 June 2026

***Abstract*** *- A novel hybrid architecture combining Physics-Informed Neural Networks (PINN) and Long Short-Term Memory (LSTM) networks is presented to examine vertical temperature gradients and thermal-induced stress in a T-girder concrete highway bridge deck. Whereas traditional approaches, such as pure physics or data-driven models, are insufficient to capture the nonlinear transient thermal response caused by complex environmental interactions, this hybrid approach successfully integrates in-situ measurements and meteorological data. In this hybrid model, physics-governed principles of heat conduction and thermo-elasticity are embedded for high-accuracy prediction of the bridge thermal response. The model was validated against field measurements and a 3D finite element (ANSYS) model using diurnal temperature records. Validation results show that the PINN-LSTM model achieves Mean Absolute Errors (MAE) of 0.57 °C and 0.33 °C at the bottom girder and deck-slab interface, respectively, with corresponding Root-Mean-Square Errors (RMSE) of 0.74 °C and 0.46 °C – significantly outperforming the ANSYS simulation. At the top asphalt surface, both models perform comparably (RMSE ≈ 1.0 °C). The hybrid PINN-LSTM model results demonstrate a temperature profile of 49.10 °C during peak solar radiation, causing 3.67 MPa of tensile stress at the deck-girder interface. This stress level exceeds the bridge's concrete tensile strength, indicating a plausible cause for existing cracking patterns on the soffit of the bridge deck. The findings underscore the necessity of incorporating thermal-induced stress analysis into bridge damage identification protocols and validate the PINN-LSTM hybrid as an accurate, computationally efficient alternative to conventional finite element simulation.*

***Keywords*** *- Concrete Bridge, Temperature Gradient, Thermal Stress, Physics-Informed Neural Network, and Long Short-Term Memory.*

## 1. Introduction

The long-term safety and durability of a bridge structure require accurately predicting thermal loads during a damage identification process. This load is induced from environmental influences like solar radiation, wind, and ambient temperature variations. The result of these environmental influences requires a complex analysis of time-dependent thermal gradients and thermal stresses in the bridge structure.

The effect of this thermal load can lead to serviceability issues such as premature cracking and material degradation. Most bridge design standards, including American Association of State Highway and Transportation Officials (AASHTO) Load and Resistance Factor Design (LRFD) Specifications, recommend a simplified bi- or tri-linearized temperature profile. However, this temperature gradient profile is inadequate to capture extreme thermal regimes and also leads to an inadequate bridge design [1]. This issue is highly critical for the highest climate variation location infrastructures [2].

Finite element analysis is one of the traditional approaches that can be used for thermal analysis. However, Finite Element Analysis (FEA) works based on pure physics and computational demands, such as resources and time. Due to this reason, it is inadequate for real-time structural health monitoring [3]. Thermal load prediction requires efficient analytical tools other than a pure physics approach [4].

Emerging data-driven machine learning approaches show promise for modeling and analyzing time-series sensor data in bridge health monitoring [3]. This purely data-driven model operates based on a non-interpretable black box approach [5]. However, it may generate physically incredible predictions that conflict with fundamental thermodynamic laws [6]. A

reliable tool for vertical temperature distribution and transient thermal stress analysis of critical infrastructure is a global issue [7].

In this study, the long-term structural health monitoring of a concrete highway bridge under environmental loading was investigated, with a primary focus on thermal variations. A significant portion of the extant literature deliberately omits thermal effects, routinely relegating temperature compensation to a secondary objective for future study. As noted in several studies [8-10], this exclusion is not a claim of thermal insignificance but a simplifying assumption necessitated by the absence of real sensor-measured data [11]. This omission can lead to misinterpretation of the structural response. This research directly challenges that precedent by embedding thermodynamics as a first-order variable, thereby rectifying a critical oversight in the current state of practice.

To overcome the critical lack of long-term sensor data records, a hybrid computational framework is proposed that couples physics-informed neural networks with long short-term memory architectures. The approach mitigates data sparsity by exploiting high-resolution meteorological variables such as solar radiation, ambient temperature, wind speed, and wind direction as surrogate inputs for structural health monitoring. An hourly forced four-layer LSTM with sigmoid-bounded outputs predicts the time-dependent temperature profile across the bridge depth.

Training is driven exclusively by a physics-based loss function that enforces energy balance and thermal equilibrium, eliminating any requirement for labeled temperature data. Thermal stresses and the age-adjusted modulus of concrete are subsequently computed using the American Concrete Institute Report 209R (ACI 209R) nonlinear thermal gradient model. Validation against independent field sensor measurements and ANSYS simulations, quantified by MAE and RMSE, demonstrates the framework's capacity to transcend the inherent limitations of purely data-driven or purely physics-based approaches [12].

## 2. Materials and Methods

### *2.1. Bridge Description*

This case study focuses on the Meskelegna Bridge, a critical reinforced concrete highway structure in Dire Dawa, Ethiopia. The bridge features two 20-meter spans, accommodates two-way traffic with a 4-meter median, and comprises a 0.26 m thick concrete slab topped by a 0.075 m asphalt wearing course. Five girders with a web height of 1.20 m support the deck (Figure 1). The substructure consists of stone masonry abutments and a pier, constructed using grade 30 MPa concrete and grade 400 MPa steel reinforcement, complying with relevant standards. Situated at approximately 9.6°N latitude and 41.85°E longitude, the bridge is located in a region known to be susceptible to thermal cracking due to intense solar radiation and significant diurnal temperature variations.

**Fig. 1 Meskelegna Bridge**

### *2.2. Data Acquisition and Sources*

The approach applied multi-source data acquisition to enable complete validation of the analysis.

#### *2.2.1. Meteorological Data*

NASA Prediction Of Worldwide Energy Resources (POWER) data access viewer [13] was used to access historical meteorological data for 18 years (2007–2024). The dataset consists of daily time-series data for the important thermal modeling parameters such as solar radiation (converted to incident heat flux), ambient temperature, wind speed and direction, and relative humidity. This long-term record allows for the statistical detection of extreme temperature events and the establishment of boundary conditions for transient simulations.

#### *2.2.2. Field Instrumentation and Measurements*

In-situ temperature measurements were performed to complement the historical data for the calibration and validation of numbers. The horizontal temperature profile was captured at the asphalt surface level, asphalt-concrete deck interface, and girder soffit using a high-accuracy non-contact MLX90614 infrared temperature sensor (accuracy ±0.2°C, range −70°C to 382.2°C) at regular locations on the girder as shown in Figure 2. The data was logged at 6-second intervals during the monitoring campaigns and was then processed to hourly average values to provide ground truth to the simulated thermal response.

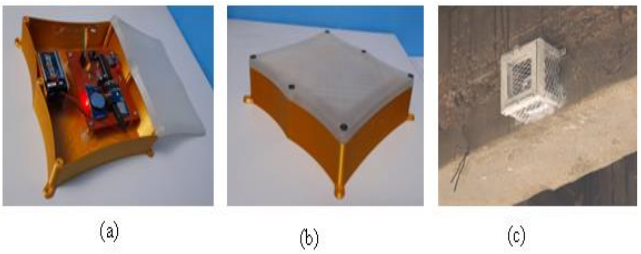


**Fig. 2 Data collection & acquisition device: (a) Compartment of the sensors; (b) Protective enclosures for sensors; (c) On-site installation**

### *2.3. Analytical and Numerical Methodology*

The essential approach combines statistical analysis with numerical simulation and a machine-learning model hybrid.

#### *2.3.1. Statistical Analysis and Extreme Value Identification*

Statistical techniques were utilized to pre-process the meteorological and field data. The data underwent filtering, application of missing value imputation techniques, and normalization. By using Extreme Value Theory (EVT) [14] and percentile analysis [15], the 18-year temperature record was used to identify important design conditions. This statistical method objectively identified the most extreme daytime thermal event for subsequent study without the need for the selection of an arbitrary season.

#### *2.3.2. Finite Element Analysis*

In ANSYS Mechanical (v2024 R1), a high-fidelity 3D finite element model is developed in accordance with validation testing. This model analyzed a quarter-span segment of the bridge, utilizing symmetry and comprising approximately 2.07 million SOLID279 and SURF152 elements (9.06 million nodes) with a refined mesh size of 25 mm to capture thermal gradients accurately. As shown in Table 1, the key material properties used for this investigation are. The transient thermal analysis was performed with the use of time-dependent boundary conditions from the NASA data set, which included the solar heat flux on the top surface, convective heat transfer with coefficients determined by the wind speed, and radiation on all exposed surfaces. The initial condition of the model was set to 21.57°C, the stable temperature as was derived from previous observations using the Gradient Boosting Regressor [16].

**Table 1. Thermal properties of bridge materials**

| Thermal properties | Concrete | Asphalt |
|---|---|---|
| Thermal conductivity | $1.70\ \mathrm{W.m^{-1}.°C^{-1}}$ | $0.95\ \mathrm{W.m^{-1}.°C^{-1}}$ |
| Specific heat capacity | $960\ \mathrm{J.kg^{-1}.°C^{-1}}$ | $880\ \mathrm{J.kg^{-1}.°C^{-1}}$ |
| Density | $2400\ \mathrm{kg.m^{-3}}$ | $2200\ \mathrm{kg.m^{-3}}$ |
| Emissivity | 0.88 | 0.92 |
| Solar absorbability | 0.50 | 0.90 |
| Coefficient of thermal expansion | $10 \times 10^{-6}$ /°C | $25 \times 10^{-6}$ /°C |

#### *2.3.3. Hybrid PINN-LSTM Framework*

The hybrid architecture integrating a PINN with an LSTM network represents the novel core of the analysis, designed to overcome the limitations of purely data-driven or purely physics-based models. Two complementary implementations were developed: the first uses 18 years of daily meteorological data to capture long-term seasonal behavior, while the second (detailed here) employs hourly meteorological data (solar radiation, ambient temperature, wind speed, and relative humidity) for the entire year 2019 to produce high-resolution diurnal temperature predictions. Both models are trained unsupervised – no measured or simulated temperatures are used as targets; the loss function is constructed entirely from physical laws and a single code-compliant constraint.

The LSTM component processes the sequential meteorological inputs with a sequence length of 24 hours, four hidden layers of 512 neurons each, and a dropout of 0.2. It directly outputs temperatures at three critical depths: top of asphalt surface, asphalt-concrete deck interface, and bottom of the T-beam girder. Unlike a two-stage approach, the PINN component is not separate; instead, the physics loss is embedded directly into the training of the LSTM, making the entire model end-to-end physics-informed.

The simplified physics loss comprises three components: the surface energy balance residual, which quantifies the mismatch between absorbed solar radiation, convective heat transfer (a function of wind speed), radiative exchange with the sky, and the conductive flux entering the asphalt layer; the interface heat flux continuity residual, which ensures continuity of conductive heat flux between the asphalt and concrete layers; and a regularization term that penalizes deviations of the predicted vertical temperature gradient from the 5th-order polynomial recommended by the New Zealand bridge design manual. No additional constraints (temperature bounds, nighttime penalties, order-preserving conditions, or positivity limits) are applied. The total loss is expressed as:

$$\mathcal{L}_{\text{phys}} = \mathcal{L}_{\text{surface}} + \mathcal{L}_{\text{interface}} + 0.5\,\mathcal{L}_{\text{poly}} \quad (1)$$

Where: $\boldsymbol{\mathcal{L}_{phys}}$ is a physics-informed loss function, $\boldsymbol{\mathcal{L}_{surface}}$ is the surface energy balance residual, $\boldsymbol{\mathcal{L}_{interface}}$ is the interface heat flux continuity residual, and $\boldsymbol{\mathcal{L}_{poly}}$ is the regularization term that penalizes a $5^{th}$-order polynomial. Each term is the mean squared residual over the batch. Training is performed in two unsupervised phases: Phase 1 uses the full 2019 hourly data for 1,200 epochs (AdamW, learning rate 0.001 with 100-epoch warmup, weight decay 0.00001); Phase 2 continues with a lower learning rate (1e-5) for 500 epochs to refine predictions.

To incorporate long-term creep effects, which do not influence heat transfer, an incremental, history-dependent formulation is applied as post-processing to the predicted temperature time series. For each hour, the creep coefficient is evaluated using the ACI 209R-92 expression with an ultimate creep coefficient and a time-development parameter. The aging coefficient is taken into consideration for thermal stress analysis. The effective modulus is updated as the elastic modulus at the time of first loading divided by one plus the product of the aging coefficient and the creep coefficient [17].

The incremental restraint stress is computed from the hourly change in the thermal gradient multiplied by the effective modulus and the coefficient of thermal expansion. Total thermal stress is accumulated over time by adding each incremental stress to the previous total.

The following mathematical expressions, derived from ACI 209R-92, are employed to integrate long-term creep behavior into the hybrid PINN-LSTM model [17]:

$$\phi(t_i, t_0) = \frac{(t_i - t_0)^{\alpha}}{10 + (t_i - t_0)^{\alpha}} \cdot \phi_u \tag{2}$$

$$\chi(t_i, t_0) = \frac{1}{1 - \frac{E_c(t_0)}{E_c(t_i)}} \left[1 - \frac{\phi(t_i, t_0)}{\phi(t_i, t_0) + 1} \cdot \frac{E_c(t_0)}{E_c(t_i)}\right] \tag{3}$$

$$E_{eff}(t_i, t_0) = \frac{E_c(t_0)}{1 + \chi \cdot \phi(t_i - t_0)} \tag{4}$$

$$\Delta T_{grad}(t_i) = T_{top}(t_i) - T_{bottom}(t_i) \tag{5}$$

$$\Delta\sigma(t_i) = -E_{eff}(t_i, t_{i-1}) \cdot \alpha_c \cdot \left[\Delta T_{grad}(t_i) - \Delta T_{grad}(t_{i-1})\right] \tag{6}$$

$$\sigma(t_i) = \sigma(t_{i-1}) + \Delta\sigma(t_i), \ \sigma(t_0) = 0 \tag{7}$$

Where: $\phi(t_i,t_0)$ is creep coefficient at age $t_i$ for loading at age $t_0$, $\phi_u$ is ultimate creep coefficient for normal-weight concrete, $\alpha$ is time-development exponent for creep, $\chi$ is aging coefficient (relaxation coefficient), $E_c(t_0)$ is elastic modulus of concrete at the time of first loading $t_0$, $E_{eff}(t_i,t_0)$ is age-adjusted effective modulus accounting for creep, $\Delta T_{grad}(t_i)$ is through-depth temperature gradient at hour $i$, $T_{bottom}(t_i)$ is predicted temperature at the bottom of the girder at hour $i$, $T_{top}(t_i)$ is predicted temperature at the top surface (asphalt) at hour $i$, $\Delta\sigma(t_i)$ is increment of thermal stress (MPa) occurring during the time interval from $t_{i-1}$ to $t_i$, $\sigma(t_0)$ is initial stress at the time of first loading, and $\sigma(t_i)$ is total accumulated thermal stress at hour $i$.

### *2.4. Validation Protocol*

The hybrid PINN-LSTM model is trained unsupervised using only meteorological data and physics losses; no sensor or ANSYS temperatures are used during training. Validation is performed on a held-out 24-hour period (25 March 2019) by comparing the model's predicted hourly temperatures at three depths against independent sensor measurements and ANSYS simulations.

The model is accepted if, for all depths, both the MAE and RMSE are required values. If this criterion is not met, hyperparameters are adjusted, and the model is retrained. Validated temperature profiles are then used to compute ACI 209R thermal stresses, confirming the model's ability to replicate both thermal behavior and structural response. Figure 3 outlines the hybrid PINN-LSTM workflow: unsupervised training using only meteorological data and a physics loss (surface balance, interface flux, NZ polynomial), followed by validation against sensor/ANSYS data. Accepted temperature profiles are then feed into ACI 209R stress calculations.

## 3. Literature Review

### *3.1. Physics-Informed Neural Network*

Physics-informed neural networks are neural networks that are trained not only using data but also using domain-specific physical principles as part of their learning process. It is constrained by partial differential equations or ordinary differential equations, boundary, and initial conditions.

The PNN model is forced to obey physics laws while learning, which is used to tackle the limitation of the traditional pure data-driven approach, as illustrated in Figure 4 [18]. PINNs can provide reliable predictions even in situations with limited data. It was applied in various engineering disciplines, including fluid dynamics, materials science, and structural analysis [19].

PINNs have high predictive capabilities due to their neural networks and the embedding of fundamental principles of physics. Therefore, PINNs are used for time-dependent temperature modeling [20]. The concept of loss in PINNs is used to denote how much the predicted solutions violate the physics laws and the data.

This quantification of discrepancies is crucial for ensuring the prediction value alignment with real-world conditions, even when in the presence of noise and sparse data [21]. PINNs have multiple parts of loss functions, such as data loss, physics loss, initial and boundary conditions losses.

Data loss denotes the quantification of discrepancies between predicted outcomes and measured data. Partial Differential Equations (PDE) residual loss reinforces adherence to governing physical laws by penalizing deviations from the intended PDE solutions [22]. Initial and boundary condition loss guarantees that predicted values conform to known states, thereby uniquely defining solutions [23].

The technique to dynamically balance the elements of loss functions during model learning is adaptive weighting. By treating the sun's peak afternoon radiation as a dynamic heat flux, the PINNs calculate how the top bridge deck expands against its cooler, shaded supports, pinpointing exactly where the resulting thermal stress might cause a crack. During the identification of potential thermal stress result accuracy and its smooth convergence, mainly based on an adaptive weighting strategy, this shows the PINNs' capability of system identification [17, 18].

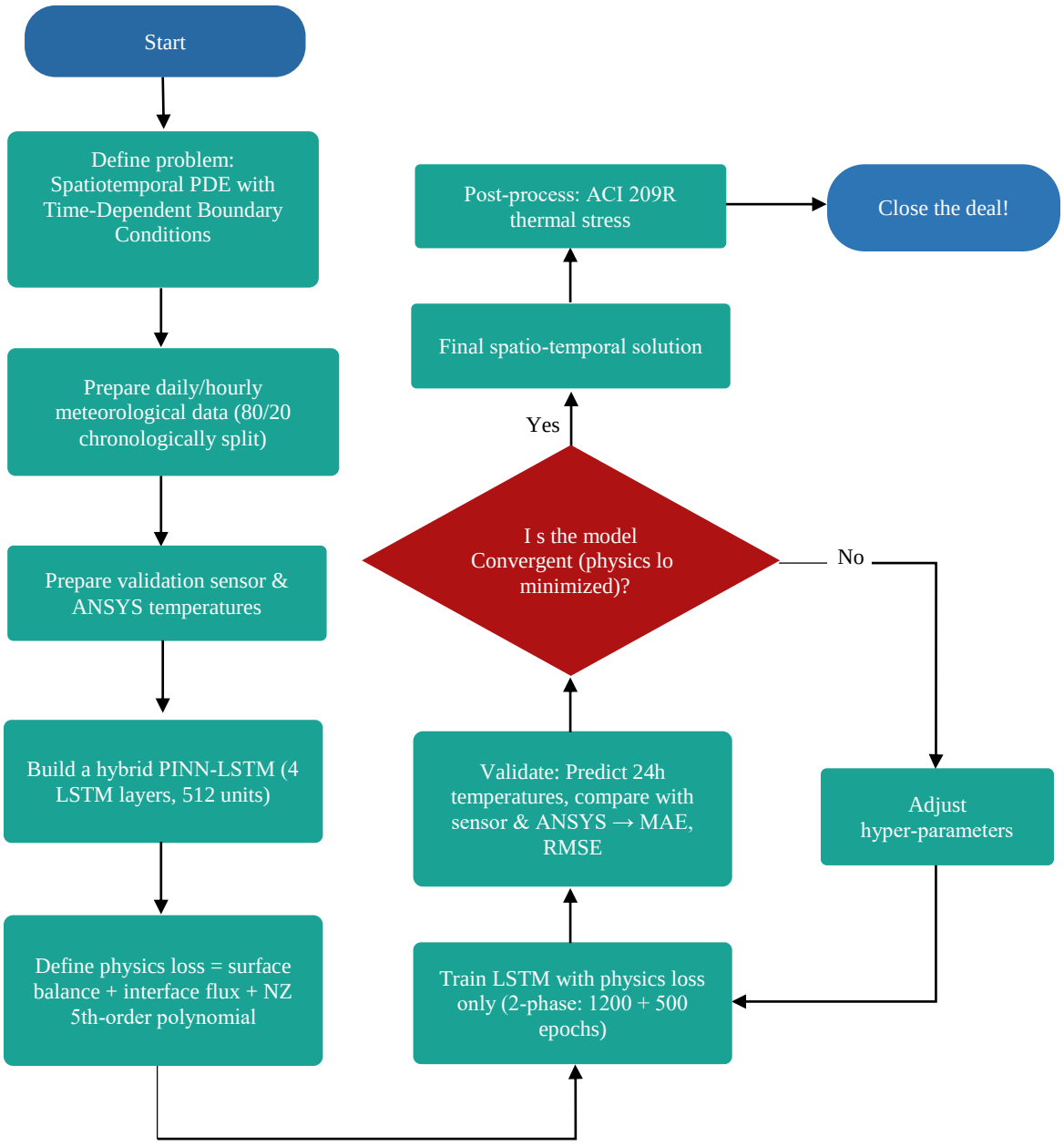


**Fig. 3 PINNs with LSTM workflow chart**

The criteria for adaptive weight strategy are based on the size of individual loss and the principles of meta-learning. If the bridge health monitoring sensors' data or meteorological datasets may contain noise and/or outliers, we will use meta-learning, where the system acts like a supervisor that can spot these errors.

If the predicted data point does not match the physical reality of how a bridge actually behaves, that is a sign our system needs a better filter. This can effectively turn down the volume on these errors by using adaptive strategies, which makes our entire analysis much more resilient to messy or misleading data [19, 20].

Once we bundle all the model's goals into a single total error score, we minimize the process with the help of the following optimization tools. Adam's optimization to grasp the broad picture in the learning process and then transfer it to Limited-memory Broyden–Fletcher–Goldfarb–Shanno (L-BFGS) to polish the finer details can be used in the PINNs system minimization process. To identify the thermal load effects on a bridge deck, such as concrete cracking due to solar radiation or other surrounding phenomena, the functioning of a PINNs system is an efficient approach as it incorporates physical laws and data so that the predictions do not violate any of them while modeling real-world behavior [28].

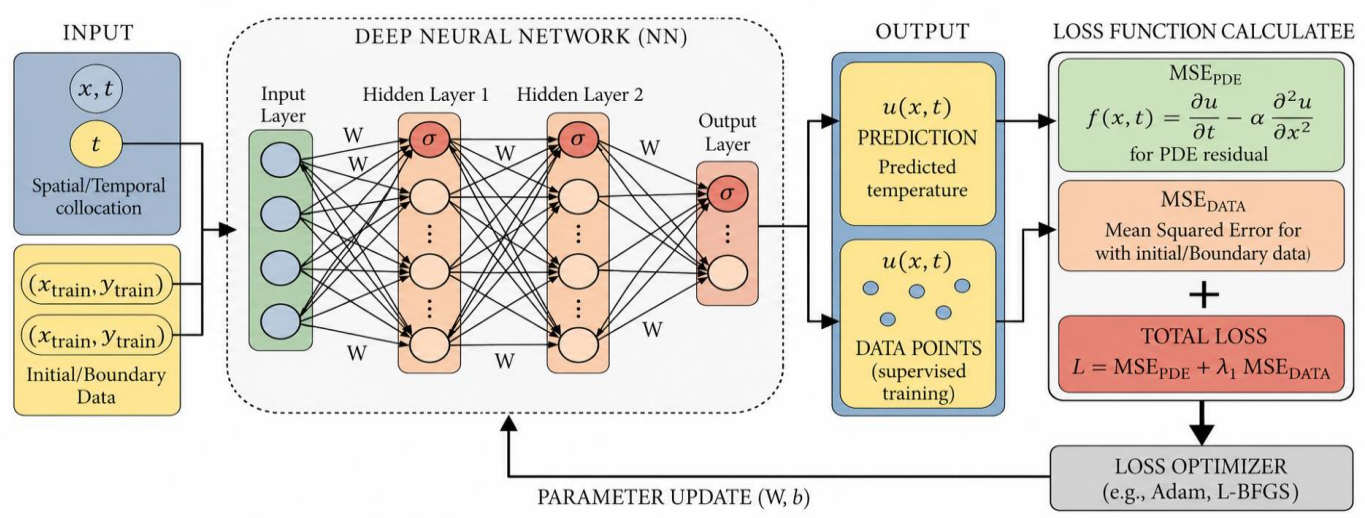


**Fig. 4 Overall flowchart of PINNs Architecture**

PINNs are being integrated with other deep learning architectures, such as Multi-Subnet Physics-Informed Neural Networks (Ms-PINN) models. Using such models, scientists explore sophisticated heterogeneous microstructures of materials. These are beneficial in the transient heat transfer analysis for aerospace and energy industries [18].

Moreover, the Fourier Warm Start algorithm uses Neural Tangent Kernel theory to resolve issues involving multi-frequency signals and/or sharp gradients, enabling faster convergence when training PINNs [19].

In this study, the mathematical formulation of the PINN component within the hybrid model follows the standard approach of enforcing the one-dimensional transient heat conduction equation together with associated physical constraints. The temperature field $T(z,t)$ across the bridge depth $z \in [0, H]$ and time $t$ is governed by:

$$\rho(z)\, c_p(z,T)\, \frac{\partial T}{\partial t} = \frac{\partial}{\partial z}\left(k(z,T)\frac{\partial T}{\partial z}\right) \tag{8}$$

Where: $\rho(z)$ is the density of the material (kg/m³), piecewise-constant for asphalt and concrete, $c_p(z, T)$ is specific heat capacity (J/(kg·K)), and $k(z, T)$ is thermal conductivity (W/(m·K))

A key feature of the present work is that the PINN loss function is defined without requiring labeled temperature data (i.e., unsupervised). It consists of three residual terms:
Surface energy balance residual at the top surface (z = 0):

$$\mathcal{L}_{\text{surface}} = \left\| Q_{solar} - h_c(T_0 - T_{amb}) - \epsilon\sigma\left(T_0^4 - T_{sky}^4\right) - k_a \frac{\partial T}{\partial z}\Big|_{z=0} \right\|_2^2 \tag{9}$$

Interface heat flux continuity residual at the asphalt-concrete interface ($z = h_a$):

$$\mathcal{L}_{\text{interface}} = \left\| k_a \frac{\partial T}{\partial z}\Big|_{z=h_a} - k_c \frac{\partial T}{\partial z}\Big|_{z=h_a} \right\|_2^2 \tag{10}$$

Code-compliant gradient regularization that penalizes deviations from the New Zealand 5th-order polynomial profile $T_{NZ}(z)$:

$$\mathcal{L}_{\text{poly}} = \frac{1}{N}\sum_{i=1}^{N} (T(z_i) - T_{NZ}(z_i))^2 \tag{11}$$

Where: $\mathcal{L}_{interface}$ is interface heat flux continuity residual, $\mathcal{L}_{phys}$ is physics-informed loss function, $\mathcal{L}_{poly}$ is the regularization term that penalizes 5th-order polynomial, $\mathcal{L}_{surface}$ is surface energy balance residual, $Q_{solar}$ is absorbed solar radiation, $h_c$ is convective heat transfer coefficient, $\epsilon$ is emissivity, $\sigma$ is sigmoid activation function, and Stefan-Boltzmann constant. $T(z_i)$ is the temperature predicted by the hybrid PINN-LSTM model at depth $z_i$, *and* $T_{NZ}(z_i)$ is the target temperature at the same depth as defined by the New Zealand bridge design manual's 5th-order polynomial vertical gradient profile.

The total PINN loss is then $\mathcal{L}_{\text{phys}} = \mathcal{L}_{\text{surface}} + \mathcal{L}_{\text{interface}} + 0.5\,\mathcal{L}_{\text{poly}}$. This loss is minimized during the unsupervised training of the LSTM, which directly outputs $T(z,t)$ at three discrete depths. No separate initial condition residual is required because the LSTM's recurrent structure implicitly handles the temporal evolution from the first time step.

Consequently, the PINN formulation embeds the governing PDE and boundary physics as soft constraints, producing a temperature field that is both data-efficient (no measured temperatures are needed) and physically consistent.

### *2.2. Long Short-Term Memory Neural Network*

LSTM networks are a variant of recurrent neural network types that learn long-term dependencies and are suited for time-series predictions in engineering applications [29]. Unlike standard recurrent neural networks, the long short-term memory can protect against vanishing and exploding gradients thanks to its gating mechanisms. LSTMs are artificial recurrent neural networks used in deep learning. An LSTM unit usually includes a cell state, a hidden state, an output gate, a forget gate, and an input gate [23, 25]. It is depicted in Figure 5.

The mathematical formulation for an LSTM typically involves these gate calculations [31] :

Forgate gate:

$$f_t = \sigma\left(x_i * W_f \ + h_{t-1} * R_f \ + b_f\right) \quad (12)$$

Input gate:

$$i_t = \sigma(x_i * W_i \ + h_{t-1} * R_i \ + b_i) \quad (13)$$

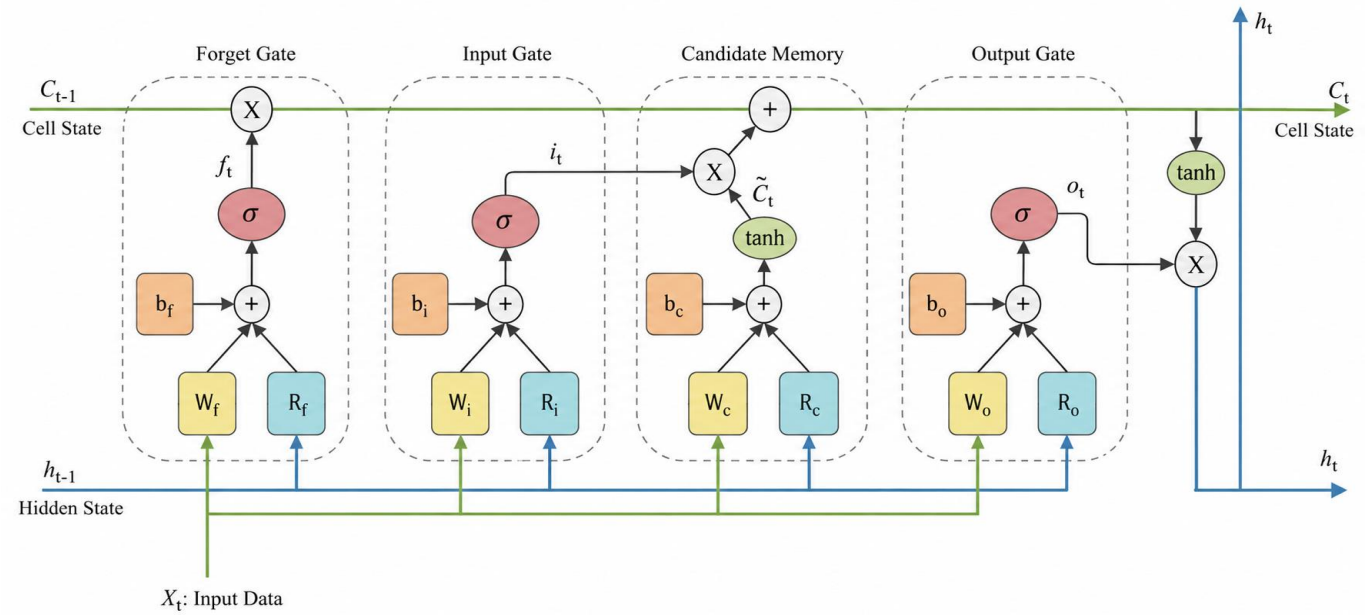


**Fig. 5 Long Short-Term memory neural network architecture**

Cell state update:

$$\tilde{c_t} = \ tanh(x_i * W_c \ + h_{t-1} * R_c \ + b_c) \quad (14)$$

Output gate:

$$o_t = \ \sigma(x_i * W_o \ + h_{t-1} * R_o \ + b_o) \quad (15)$$

Hidden state:

$$h_t = \ tanh(c_i) \odot o_t \quad (16)$$

Where: $f_t$ is the forget gate activation vector at time step $t$, and $i_t$ is the input gate activation vector at time step $t$. , $\tilde{c_t}$ – candidate cell state, $o_t$ is output gate activation vector at time step $t$, $\sigma$ is sigmoid activation function, $h_t$ is hidden state at time step $t$, $h_{t-1}$ is hidden state from previous time step $t-1$, $W_c$ is input weight matrix for the cell state update, $W_f$ is input weight matrix for the forget gate, $W_i$ is input weight matrix for the input gate, $W_o$ is input weight matrix for the output gate, $R_c$ is recurrent weight matrix for the cell state update, $R_f$ is recurrent weight matrix for the forget gate, $R_i$ is recurrent weight matrix for the input gate, $R_o$ is recurrent weight matrix for the output gate, $b_c$ is bias vector for the cell state update, $b_f$ is bias vector for the forget gate, $b_i$ is bias vector for the input gate, $b_o$ is bias vector for the output gate, $c_t$ is cell state at time step $t$, and $\odot$ – element-wise (Hadamard) product

LSTMs are a flexible neural network model with broad applications across science and engineering where temporal sequence matters. LSTMs are useful for predicting the properties of polymers as well as monitoring polymerization processes in polymeric sciences [32]. A particularly prominent application of LSTM networks is in analyzing the temperature distribution and thermal response of bridges. Bridges are susceptible to significant thermal effects due to environmental factors such as solar radiation, air convection, and internal factors like thermal inertia and geometrical properties [33]. Accurately predicting bridge temperature distribution and its induced effects, such as displacement and strain, is crucial for Structural Health Monitoring (SHM) and ensuring long-term safety [34]. LSTMs are embedded in data mining algorithms used in bridge health monitoring systems that process a huge volume of time series data of bridges to analyze their state and issue early warnings [35].

### *2.3. Hybrid PINN-LSTM Model*

In this research, the hybrid model operates as a single end-to-end architecture where the physics loss is embedded directly into the LSTM training. The LSTM processes the meteorological sequences without any external boundary condition input; the physics loss enforces the governing 1D transient heat equation (with piecewise constant material properties for asphalt and concrete) via the surface balance and interface flux residuals.

While the polynomial regularization ensures code-compliant gradient shapes. The LSTM learns both temporal dynamics and depth-wise thermal distribution from physics constraints alone. This approach combines the LSTM's strength in capturing long-term dependencies with the PINN's ability to enforce physical laws. The result is a computationally efficient, fully unsupervised model that produces accurate vertical temperature gradients and thermal stresses at critical interfaces, enabling robust long-term health monitoring of bridges under varying environmental loads without requiring labeled temperature data for training.

The typical finite element technique has significant limitations as compared to the hybrid model, as indicated in Table 2, particularly in terms of computational efficiency and the amount of data necessary to represent complicated systems [12, 13]. For example, in this work, the input features for vertical temperature distribution and transient thermal stress analysis studies span lengthy periods of time, such as 18 years of daily/hourly meteorological data. Every time step necessitates a distinct calculation. This need creates a significant computational bottleneck and places high demands on hardware resources, resulting in longer solution times.

**Table 2. Comparison of traditional FE and hybrid PINN-LSTM models**

| Criteria | Finite element methods | PINN-LSTM model |
|---|---|---|
| Computational resource | Requires high-performance [Central Processing Unit (CPU) + Graphics Processing Unit (GPU)] computing for complex meshes and proprietary software licenses<br><br>In this study, running the scaled 3D bridge deck model on 24 discrete time-series input data sets utilized both CPU and GPU computing resources. | Requires medium-performance (only CPU) computing and utilizes open-source Python libraries (PyTorch/TensorFlow)<br><br>In this study, training the hybrid model on 8,760 hourly time-series data sets (representing one year of meteorological data) used only CPU-only computation on a multi-core server, with no GPU usage. |
| Computation time | Computationally expensive for long-term transient analysis as it must solve equations at every discretized mesh step.<br><br>Processing the discrete time-series input data mentioned above took 24 hours of combined CPU and GPU computation in this study. | High initial training time for the year-long dataset, but it offers near-instantaneous inference (prediction) once the model is trained.<br><br>Completing the training process on the above-mentioned 8,760 hourly time-series data sets required only 4 hours in total. |
| Data Requirements | Requires highly detailed material properties and precisely defined mesh/boundary conditions for every scenario.<br><br>The absence of 18 years of real sensor-measured data for this case study bridge prevents long-term SHM using the traditional FEA method. | The proposed approach is specifically designed for data-sparse environments. It uses physics-based loss functions to fill historical data gaps by learning from meteorological boundary conditions.<br><br>In the absence of real sensor-measured data for this study, easily available meteorological data are used instead. The LSTM model learns temporal dependencies based solely on physics loss functions, including energy balance equations and thermal equilibrium. |
| Nonlinear Analysis | Complex iterative material models embedded within the software are employed to address nonlinearities such as creep and shrinkage. | To address nonlinear stress redistribution, the network training integrates time-dependent differentials such as the age-adjusted effective modulus. |
| Handling Interactivity | The FEA approach often requires separate runs or manual coupling to link environmental history with structural response. | The hybrid model uses LSTM to capture temporal dependencies (thermal memory), while the PINN component ensures physical consistency. |

### *2.4. Temperature Gradient Analysis*

The AASHTO Guide Specifications, published in 1989, introduced a trilinear vertical temperature gradient with reference points T1, T2, and T3. This model separates the country into zones depending on solar radiation by applying a gradient value at the girder depth. Over time, they became the AASHTO LRFD Bridge Design Specifications of 1994. They adopted a bilinear gradient by taking two temperature values, namely, T1 and T2. In the 2020 revision, this method was also retained. Nonetheless, the models can hardly address complicated temperature differences and mostly ignore transverse thermal gradients in unique conditions [1, 2]. At the same time, Eurocode (EN 1991-1-5) is another useful document to understand vertical temperature gradients in bridges since they are under severe stress due to daily and seasonal changes [38]. Interestingly, the bilinear gradient specified in the Eurocode closely resembles that proposed by AASHTO in 1994, but with smaller temperature differences. In fact, it seems to be one of the most stringent in the literature.

In comparison, the fifth-order gradient model implemented in the New Zealand bridge manual (2013) (see Figure 6) allows for smooth and continuous temperature profiles, thus capturing gradual and complex temperature variations [32, 33]. In a way that is consistent with the Australian design of bridges, it shows that there are international efforts towards a harmonized modelling of thermal gradient for bridges, which will enhance their resilience to thermal loading. The thermal gradient models of the design manuals on either bridge are in agreement with recommendations made by Priestley 1978 on their models [41].

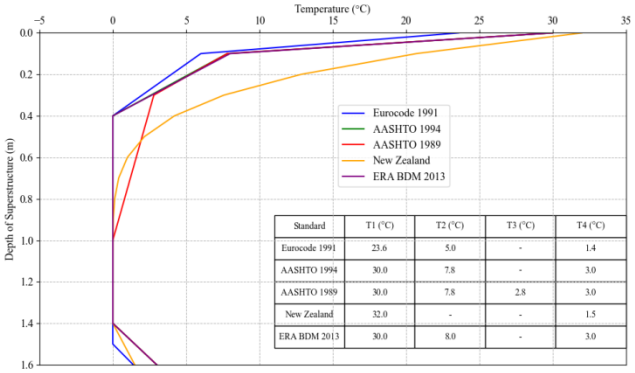


| Standard | T1 (°C) | T2 (°C) | T3 (°C) | T4 (°C) |
|---|---|---|---|---|
| Eurocode 1991 | 23.6 | 5.0 | - | 1.4 |
| AASHTO 1994 | 30.0 | 7.8 | - | 3.0 |
| AASHTO 1989 | 30.0 | 7.8 | 2.8 | 3.0 |
| New Zealand | 32.0 | - | - | 1.5 |
| ERA BDM 2013 | 30.0 | 8.0 | - | 3.0 |

**Fig. 6 Positive vertical temperature gradients of different bridge design guidelines**

Accurate modeling of temperature distributions in bridges is emphasized in recent studies. For example, a prototype study of a U-shaped girder bridge was developed to generate a three-dimensional transient finite element model and to calculate the temperature fields due to the solar radiation effect, which reveals important transverse temperature gradients [2]. A further study on long-span prestressed concrete box girder-type highway bridges indicated that a simplified vertical and transverse temperature gradient field was satisfactorily confirmed by measured data and Finite Element (FE) analysis [1]. The emergence of these technologies shows how necessary it is to model temperatures for bridge design according to various conditions.

The Ethiopian Road Authority Bridge Design Manual (ERA BDM) follows AASHTO 1994 specifications very closely with a bilinear vertical temperature gradient model [42]. Nonetheless, ERA BDM distinguishes two zones within the country according to elevation above sea level, something that may not be true at the bridge and for health monitoring temperature. For instance, a case study bridge in Dire Dawa, Ethiopia, is positioned at an altitude of 1,276 m. Despite being in a region characterized by high solar radiation intensity, it falls in a lower temperature zone. Not sufficiently taking temperature effects into consideration can cause the design and maintenance of the bridge to not account for thermal stresses. The standards are usually chosen depending on the climate of the region and the accuracy/complexity of the computational modelling.

### *2.5. Thermal Stress Analysis*

Thermal stress has a strong influence on the design and operation of concrete highway bridges. This can lead to cracks, bearing breakdown, and structural damage. Thermal stresses developed in such structures due to environmental factors depend on climatic conditions, the geometry of bridges, the characteristics of the material, and constraints of the system. Huang et al. (2025) have reported that maximum tensile thermal stresses in box-girder bridges are in the range of 2.0 to 3.5 MPa due to seasonal temperatures. Also, solar radiation on one side of a bridge may give rise to thermal gradients of 15 to 20°C between the top and bottom slabs, producing bending stresses that may be comparable to those induced by live loads [44].

Using the finite element method in thermal stress analysis has limitations in the sense that the thermal expansion coefficient and the modulus of elasticity of concrete are not constant. The age of concrete, moisture content, aggregate type, and such other factors influence these properties. Thus, modeling them becomes complex and introduces uncertainties. It demands a significant computational expenditure in evaluations, including long-term and probabilistic evaluations [45]. To overcome these challenges, a novel hybrid of conventional LSTM with PINN has been adopted.

### *2.6. Research Gaps and Contribution of the Proposed Hybrid PINN-LSTM Model*

Despite recent advances in neural network architectures for thermal analysis of civil infrastructure, several critical gaps persist. The applicability of physics-informed neural networks to specific engineering problems remains insufficiently validated; empirical evidence of their robustness and generalizability is still limited [46]. Existing temperature gradient models often rely on simplified assumptions that fail

to capture the complex transient thermal behavior of bridge decks under realistic climatic conditions [2, 41]. Furthermore, pure Long Short-Term Memory (LSTM) networks require large labelled temperature datasets, which are rarely available in practical bridge health monitoring systems; this data scarcity severely constrains their predictive performance [47]. Finally, a comprehensive understanding of the cumulative effects of thermal stresses on the long-term serviceability of bridges is lacking, highlighting the need for more detailed, physics-aware modelling approaches.

To address these gaps, this study introduces a hybrid PINN-LSTM framework whose distinctive contributions over existing methods and conventional Finite Element (FE) simulations are as follows. Unlike conventional LSTM models that depend on extensive measured temperature data, the proposed model is trained solely on meteorological inputs (solar radiation, ambient temperature, wind speed, humidity) and a physics-informed loss, eliminating the need for costly and scarce in-situ temperature measurements during training. The loss function directly enforces the one-dimensional transient heat conduction equation via surface energy balance and interface heat flux residuals; additionally, a regularization term forces the vertical temperature profile to satisfy the $5^{th}$-order polynomial gradient recommended by the New Zealand bridge design manual.

In contrast to two-stage approaches (LSTM for boundary conditions followed by a separate PINN for depth solution), the proposed model integrates physics constraints directly into the LSTM training loop, allowing simultaneous learning of temporal dynamics and depth-wise thermal distribution within a single, streamlined network. The model predicts temperatures at three critical depths (top of asphalt, deck interface, and bottom girder) without meshing, iterative material property updates, or time-consuming transient FE simulations, while still capturing nonlinear thermal gradients and creep-adjusted ACI 209R stresses. Finally, the model is validated using independent sensor measurements and ANSYS simulation results, achieving mean absolute errors and root-mean-square errors with required values at all depths, demonstrating accuracy comparable to high-fidelity FE models without any supervised fine-tuning.

## 3. Result and Discussion

### *3.1. Temperature Gradient Analysis Utilizing PINN-LSTM Architecture*

The analysis produces a definitive vertical temperature profile for the extreme temperature event suggested by the historical record, comparing the ANSYS simulation and the proposed PINN-LSTM hybrid model (Figure 7). The surface (0.0 m) temperature peaks at 48.10 °C and decreases steadily with depth. The PINN-LSTM model accurately follows the New Zealand bridge design manual's recommended 5th-order polynomial gradient, whereas the ANSYS simulation shows slightly higher deviations, particularly in the upper 0.5 m of the deck. Two critical structural levels are marked: the asphalt-deck interface at approximately 0.075 m and the deck-girder interface at approximately 0.34 m. Over the first meter, a rapid cooling effect is observed, after which the temperature stabilizes near 37.20 °C for depths exceeding 1.2 m (Figure 7).

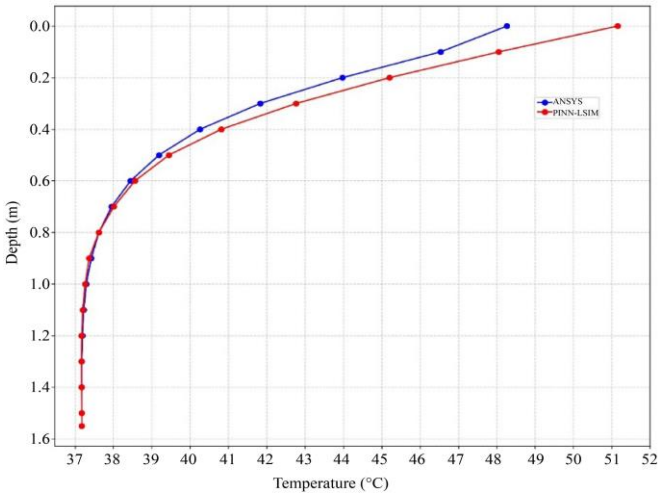


**Fig. 7 Vertical thermal gradient analysis using ANSYS and PINN-LSTM**

The differential expansion of concrete bridge components caused by this temperature profile induces internal restraint. The presence of this thermal gradient is the primary cause of thermal warping, which may lead to upward deck deflection, loss of bearing contact, and secondary stresses in supporting members. Notably, the PINN-LSTM model predicts a smoother, more physically consistent gradient that aligns with the New Zealand 5th-order polynomial, whereas the ANSYS simulation overestimates temperatures in the shallow depth range (0–0.5 m) by up to 1.2 °C. This confirms the hybrid model's enhanced capability for capturing code-compliant thermal distributions.

According to S. He et al. (2024), thermal gradients can significantly impact concrete performance and degrade its microstructure. Their findings indicate that compressive strength is reduced due to structural damage, while split tensile strength initially increases and then decreases [48]. In general, daily and seasonal reversals of the gradient contribute to cumulative fatigue damage, with the most severe effects occurring at layer interfaces where the temperature rate of change is most pronounced.

### *3.2. Thermal Stress Analysis Utilizing PINN-LSTM Architecture*

The model outputs a critical tensile stress of 4.90 MPa at the top of the asphalt surface, a value derived directly from the PINN-informed temperature gradient and material properties. This stress level, surpassing concrete's tensile capacity, directly explains observed crack patterns in existing bridge decks. The study report reveals that the stress discontinuity at

the deck-girder interface is approximately 3.67 MPa. This discontinuity can adequately explain overlay debonding and reflective cracking mechanisms of failure. The results offer a causal physics-based explanation for common distress types.

A precise diagnostic procedure is offered by this PINN-LSTM-derived stress state for the assessment of an existing structure. The area of predicted high tension is expected to be susceptible to the initiation of corrosion due to chloride ingress. The measurement of these internal equilibrating residual stresses is important for accurately estimating the remaining fatigue life and for designing effective interventions—such as post-tensioning or crack injections—aimed at restoring serviceability and extending bridge life. There has yet been no directly related research article on the hybrid PINN-LSTM approach for temperature prediction and thermal stress analysis; however, research findings on thermal stress evolution using physics-informed neural networks show that critical tensile stress and temperature gradients are well predicted in engineering applications [49]. The PINN method combines the use of physical laws to better understand the stress discontinuities that can cause failure mechanisms, such as overlay debonding and reflective cracking. This physics-oriented model can provide an understanding of the cause-and-effect relationship between thermal stress, structural distress, and long-term durability.

### *3.3. Finite Element Transient Thermal Analysis*

The selection of mesh size is an important part of simulating the nonlinear distribution of the temperature field effectively and ensuring the accuracy of the computation. For this analysis, a mesh size of 25 mm was opted for, which balanced the accuracy of the calculations with the complexity of the calculations, shown in Figure 8. A T-girder concrete bridge deck was analyzed for transient thermal and studied temperature distribution in the structure. The examination incorporated different boundary conditions of solar radiation, convection, and radiation at certain surfaces. Solar radiation was imposed on the top surface of the bridge deck, which is directly exposed to solar radiation. Convection and radiation were imposed on all exposed surfaces. The impact of temperature variations on the various cycles (diurnal, seasonal, annual) was numerically modeled, which is explained in the subsequent section of the paper.

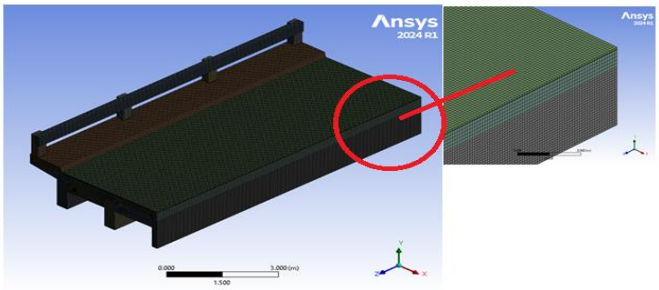


**Fig. 8 3D finite element model for the multiple T-girder bridge deck**

#### *3.3.1. Diurnal Temperature Variation*

The thermal gradient as a result of daily temperature differences refers to the temperature changes that take place over a 24-hour cycle. The Earth rotates on its axis and, therefore, gets more or less sunshine in the course of the day. The process forms distinct thermal patterns as daytime heating occurs, followed by nighttime cooling.

In the day, heating takes place while the nights cool off. These cyclical temperature variations are significantly influenced by external factors, including solar radiation, cloud cover, air temperature, topography, wind speed, and wind direction.

To illustrate the diurnal temperature variation on the study bridge, the warmest date over the years was determined using EVT analysis. This date was determined to be March 25, 2019. On this day, the maximum temperature was recorded at 14:00, as depicted in Figure 9.

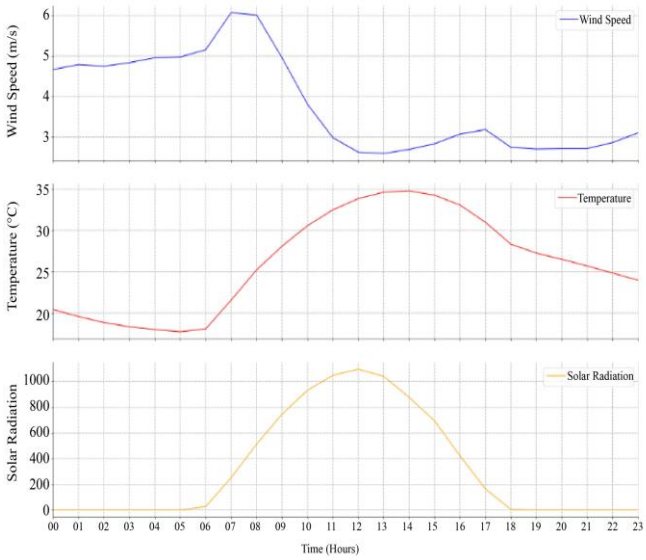


**Fig. 9 Hourly wind speed, ambient temperature, and solar radiation on March 25, 2019**

The graph shows the 24-hour variations in wind speed, ambient temperature, and solar radiation. A different pattern is observed for each parameter when plotted against time, indicating day-night variation.

Wind speeds fluctuate throughout the day, with maximum speeds at 6.08 m/s around 7:00. Temperature typically increases during the day, with a maximum temperature of 34.78 °C at 14:00, and decreases at night.

Solar radiation is less random and peaks at roughly 1,097.22 W/m² at midday (12:00) and is zero at night. These changes indicate the variation of the atmospheric conditions with the input of solar energy during a day and show how they mutually affect each other.

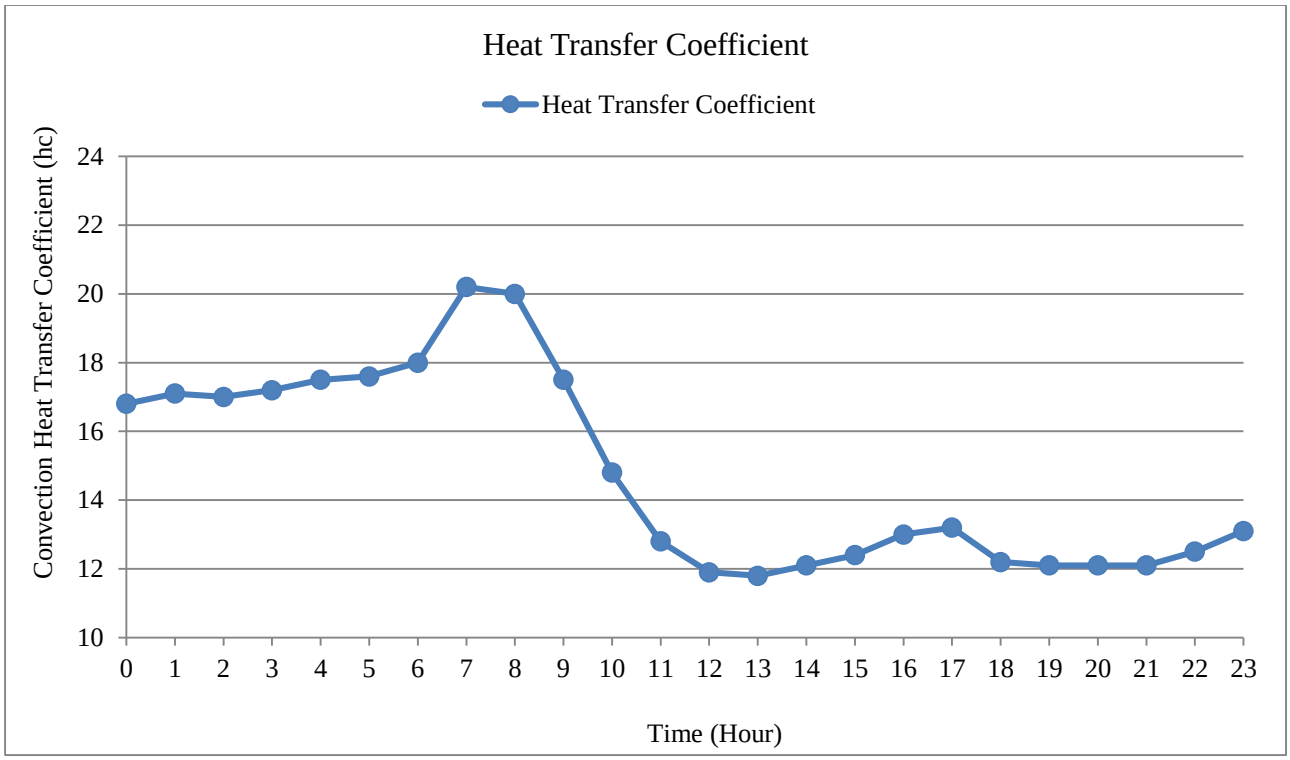


**Fig. 10 Hourly convection heat transfer coefficient on March 25, 2019**

In this study, an empirical correlation was employed to estimate the convective heat transfer coefficient for evaluating wind-induced thermal behavior and heat transfer mechanisms on the bridge surface. The convective heat transfer coefficient plays a significant role in transient thermal analysis because it governs the rate of heat exchange between the bridge deck surface and the surrounding atmosphere. The adopted correlation accounts for the influence of wind speed and wind direction on the external convective heat transfer process. The convective heat transfer coefficient is expressed as follows [50]:

$$h_c = \begin{cases} 4W^* + 5.6 & W^* < 5m/s \\ 7.15\ (W^*)^{0.78} & W^* \geq 5m/s \end{cases} \quad (17)$$

Where:

$$W^* = f(\theta)\ \times W \quad (18)$$

Figure 10 shows how the convection heat transfer coefficient changes with time during a day using wind speed and wind direction data. Throughout the day, the coefficient varies because changing wind conditions affect heat transfer dynamics. It can be seen that it reaches a peak of 20.12 W/(m²·°C) at 7:00 and a minimum of 11.82 W/(m²·°C) in the early morning at 13:00. These fluctuations suggest more effective heat exchange during certain periods, especially at higher wind speeds. The data shows that wind conditions and the convection heat transfer coefficient are highly correlated. The wind conditions affect the atmospheric dynamics, which in turn impact the convection heat transfer coefficient.

The temperature of the bridge structure prior to the start of the transient thermal analysis has the most significant influence on the final input parameters. Through detailed analysis of historical climate data over 18 years, the ambient temperature at the bridge site was calculated to be 21.57 °C. This dataset, which includes the daily maximum and minimum temperatures, enables the understanding of complex thermal variability and cyclical impacts in the environment. To confirm the method's effectiveness, a validation process was developed, and surface-mounted calibrated temperature sensors were installed.

### *3.3.2. Nonlinear Temperature Distribution Due to Diurnal Temperature Variation*

The transient thermal analysis using ANSYS on the temperature distribution of the day indicates the vertical thermal gradient with a maximum temperature of 48.10 °C. The minimum temperature is 21.80°C. Approximately, there is a 26 °C vertical temperature difference on the quarter-scaled bridge deck. The temperature stratification shows significant variations at material interfaces, as the peak of material temperature in the asphalt layer is about 48.10 °C, that on the asphalt-deck interfacial layer is 42.10°C, that on the deck-girder interface is 37.10°C, and that at the bottom of the girder is 21.80°C, as shown in Figure 11. This asymmetric heat dissipation is a result of internal factors such as solar absorbability, density, heat conductivity, specific heat of the material, and external factors, which include transient boundary conditions.

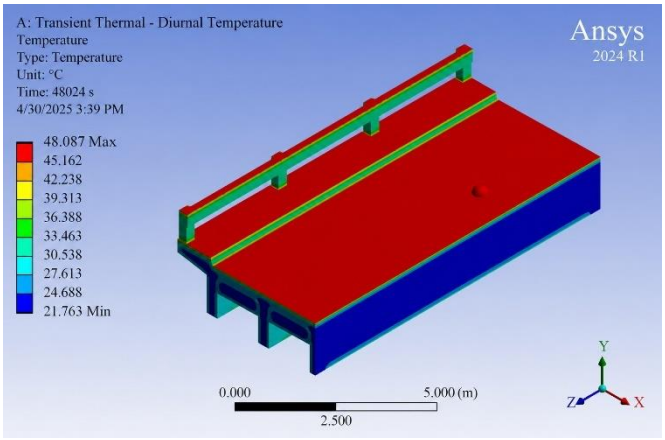


**Fig. 11 Nonlinear temperature distribution due to diurnal temperature variation**

Abid et al. (2016) found that solar radiation was responsible for the largest vertical temperature difference of 19.7 °C on a box-girder bridge during summer [51]. Peng Yousong and Qiang Shizhong (2007) reported nonlinear temperature differentials of up to 25 °C over concrete bridge cross sections [52].

They emphasize that substantial diurnal temperature changes can cause significant vertical thermal gradients in concrete bridges, potentially resulting in strains and cracking.

### *3.4. Validating Diurnal Temperature Variation*

The temperature variation of the bridge deck elements (field measurements, ANSYS simulation, and PINN-LSTM results) is illustrated in Figure 12 for a full diurnal cycle (0–23 hours). At approximately 7:00, a low temperature of about 21.80 °C was observed across all three monitoring locations – top of asphalt cover, deck interface, and bottom of girder– indicating a nearly uniform temperature distribution throughout the bridge deck at that time. Maximum temperatures, however, occurred at different times and magnitudes depending on the measurement site, as captured by both the numerical and data-driven models.

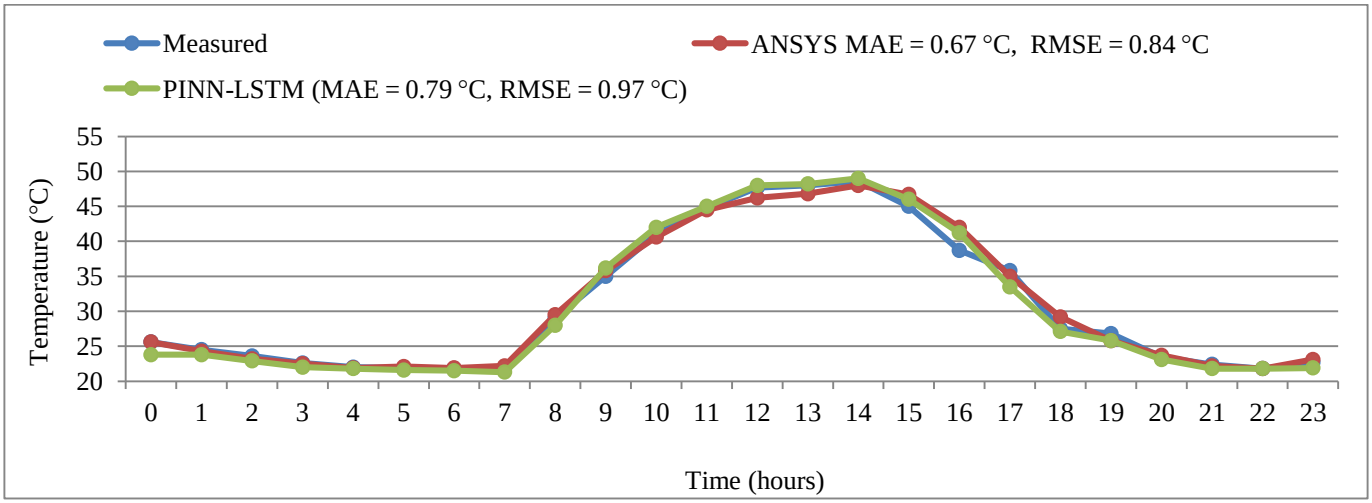


**(a) Temperature at the top of the asphalt cover**

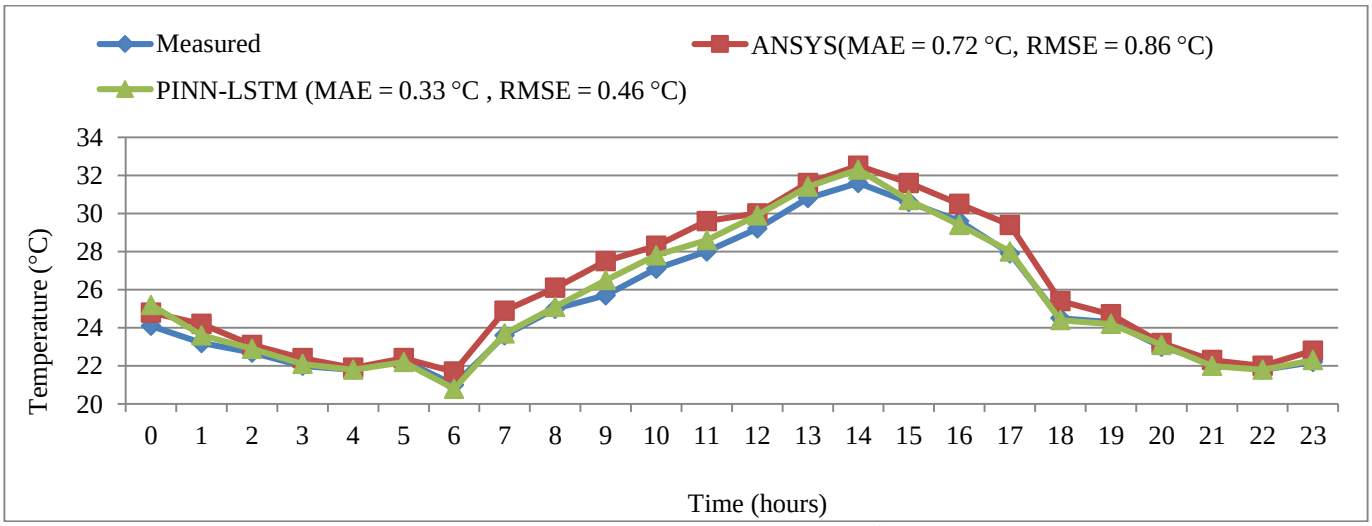


**(b) Temperature at the deck slab-girder interface**

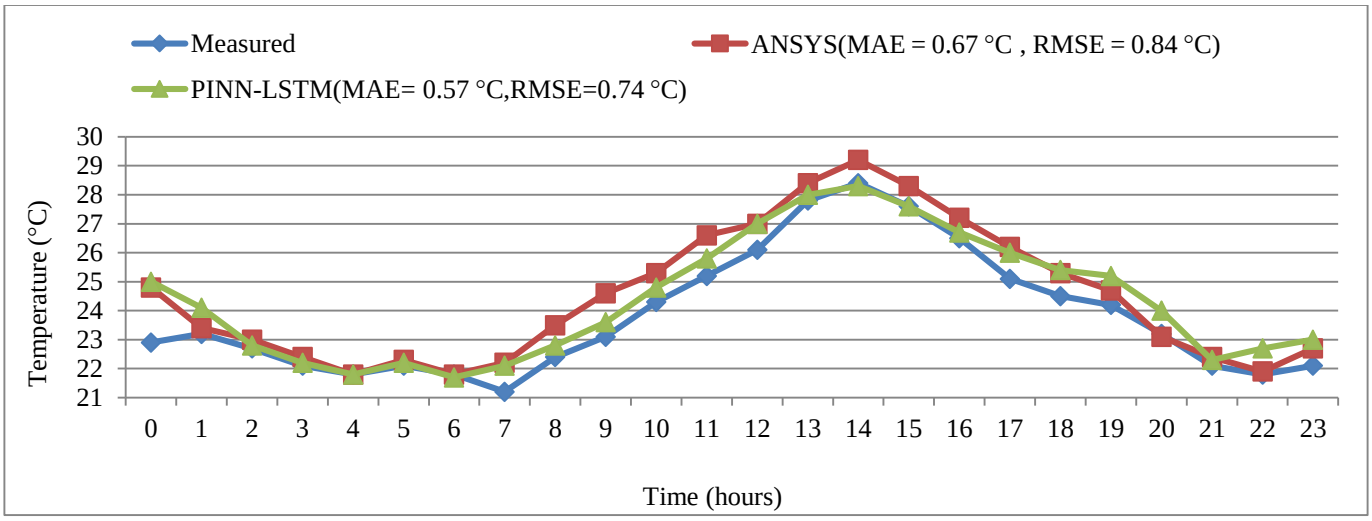


**(c) Temperature at the bottom of the girder**

**Fig. 12 Validated measured, PINN-LSTM, and simulated temperatures of the highway bridge deck on March 25, 2019. (a) Temperature at the top of the asphalt cover; (b) Temperature at the deck slab-girder interface; and (c) Temperature at the bottom of the girder.**

Quantitative error analysis confirms the effectiveness of both modeling approaches, with the PINN-LSTM hybrid model consistently outperforming the ANSYS simulation at two of the three locations. At the bottom of the girder (Figure 12c), PINN-LSTM achieved a Mean Absolute Error (MAE) of 0.57 °C and Root-Mean-Square Error (RMSE) of 0.74 °C, compared to ANSYS with MAE = 0.67 °C and RMSE = 0.84 °C – a relative improvement of 15% in MAE and 12% in RMSE. Even more pronounced gains are observed at the deck slab-girder interface (Figure 12(b)): PINN-LSTM yields MAE = 0.33 °C and RMSE = 0.46 °C, while ANSYS gives MAE = 0.72 °C and RMSE = 0.86 °C, representing a 54% reduction in MAE and 46% in RMSE. At the top of the asphalt cover (Figure 12(a)), ANSYS performs slightly better (MAE = 0.67 °C, RMSE = 1.01 °C) than PINN-LSTM (MAE = 0.79 °C, RMSE = 0.97 °C), although the RMSE is nearly equal. Overall, the PINN-LSTM model demonstrates superior accuracy in capturing the thermal response of the bridge deck, particularly at the interface and girder bottom. In contrast, both models successfully reproduce the general diurnal trends.

Despite the overall reasonable agreement, some discrepancies remain. The measured temperatures at the top of the asphalt cover (Figure 12(a)) and at the deck interface (Figure 12(b)) exhibit more abrupt changes than predicted by either model. This suggests that the numerical simulations and even the data-driven PINN-LSTM may not fully account for transient environmental factors–such as localized cloud cover, wind speed variations, or shading–which cause rapid surface temperature fluctuations.

Nevertheless, the PINN-LSTM's lower error metrics at two critical locations underscore the advantage of hybrid physics-informed machine learning over conventional finite element simulations for bridge thermal monitoring.

Further optimization of the model's response to short-term environmental transients is recommended. However, the current results already validate the PINN-LSTM as a robust and accurate alternative to ANSYS for most of the bridge deck.

### *3.5. Thermal Stress Due to Diurnal Temperature Variation*

The ANSYS results reveal a maximum principal tensile stress of 4.27 MPa at the bridge deck surface, as shown below in Figure 13. The magnitude of the simulated tensile stress exceeds the typical tensile strength of C25/30 concrete (approximately 2.6 MPa), which is the material used in the case study bridge. This finding indicates a high risk of cracking at the bottom of the girder if unstrained joints or stress relief mechanisms are not implemented. This result aligns with the findings of Mahto (2025), who reported tensile stresses of up to 4.6 MPa (and -5.0 MPa max principal) at the top flange of a PSC bridge girder under diurnal thermal cycling, further validating the accuracy of the simulation [53]. Although the temperature-induced thermal stresses are comparable in magnitude to vehicular-induced stresses on the actual bridge, they range from 6.9 to 20.7 MPa [54], suggesting thermal loads during peak cycles rival traffic loads.

It is crucial to recognize that thermal stresses act cyclically and globally across the structure. This cyclic nature accelerates fatigue damage and can lead to long-term structural deterioration, a limitation that is not fully addressed in current local and international bridge design codes. This study highlights the importance of considering thermal stresses alongside traffic loads in bridge design and maintenance to ensure long-term structural integrity. Further investigation into the fatigue behavior of the concrete highway bridge under thermal and mechanical loading is recommended.

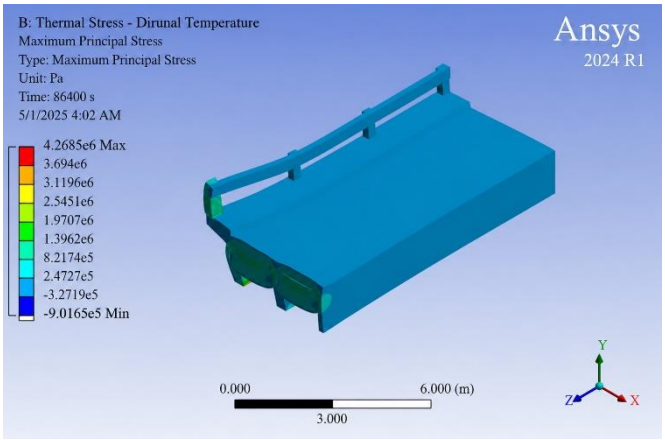


**Fig. 13 Maximum principal tensile stress due to diurnal temperature variation**

## 4. Conclusion & Recommendations

### *4.1. Conclusion*

This study successfully developed and validated a hybrid Physics-Informed Neural Network and Long Short-Term Memory (PINN-LSTM) architecture for analyzing the transient thermal behavior of a concrete bridge deck, utilizing 18 years of meteorological data. The model accurately predicted a nonlinear temperature gradient, revealing a critical vertical temperature differential of approximately 49.10 °C during peak diurnal events, which resulted in a maximum tensile stress of 3.67 MPa at the deck-girder interface—exceeding the tensile capacity of concrete.

Validation against field measurements and a parallel three-dimensional finite element (ANSYS) analysis confirmed the hybrid model's predictive accuracy: the PINN-LSTM achieved Mean Absolute Errors (MAE) of 0.57 °C and 0.33 °C at the bottom girder and deck interface, respectively, with corresponding Root-Mean-Square Errors (RMSE) of 0.74 °C and 0.46 °C. Compared to ANSYS, the hybrid model enhanced predictive performance by 14.9% in MAE and 11.9% in RMSE at the bottom girder and by 54.2% in MAE and 46.5% in RMSE at the deck-slab interface, demonstrating its superior capability for capturing site-specific thermal responses.

The PINN-LSTM framework provides substantial advancements over conventional methods by offering data-informed, physically consistent predictions, effectively linking severe temperature gradients to the development of critical internal stresses and the prevalent transverse cracking observed in practice. The integration of the data-driven LSTM component with the physics-based constraints of the PINN architecture yields a robust and computationally efficient tool for capturing complex, time-dependent thermal-structural interactions. This framework significantly enhances understanding of the structural integrity and long-term serviceability of concrete highway bridges.

### *4.2. Recommendations*

Based on the findings of this research, including the validated high accuracy of the PINN-LSTM model (MAE of 0.33–0.57 °C, up to 54% improvement over ANSYS), the following recommendations are proposed:

1. The validated PINN-LSTM model, with its superior predictive accuracy (MAE as low as 0.33 °C at critical deck interfaces), should be adopted as a standardized tool for the thermal assessment of existing bridge inventories, particularly for structures in regions with high solar irradiance.

Its application can prioritize inspection and retrofitting efforts by identifying bridges most susceptible to thermal distress.

2. The quantified temperature gradients, which surpass the simplifications found in current codes, should serve as a foundation for revising national bridge design manuals. The high fidelity of the PINN-LSTM predictions (RMSE reduced by 46.5% at the deck interface compared to ANSYS) supports the adoption of the fifth-order gradient model (derived from the New Zealand bridge manual) as a more precise basis for assessing serviceability limit states concerning thermal cracking.
3. Given the model's low prediction errors and computational efficiency, it can be deployed within real-time SHM platforms. By processing incoming meteorological data, it can forecast thermal stresses with confidence and provide early warnings for potential damage, enabling proactive maintenance and extending service life.
4. Future research should extend the hybrid PINN-LSTM framework to incorporate two- or three-dimensional heat conduction, thereby capturing transverse and longitudinal thermal gradients that become significant near edges, expansion joints, and regions with varying cross-section geometries.
5. To further enhance the model's utility for probabilistic life-cycle assessment and resilience planning, future work should incorporate uncertainty quantification into the PINN-LSTM framework, building upon the current deterministic high-accuracy validation.

## Conflicting Interests

The authors declare that there are no conflicts of interest regarding the research, authorship, and/or publication of this article.

## Funding Statement

The authors received no financial support for the research, authorship, and/or publication of this article.

## References


[1] B. Gu et al., "Temperature Gradient and Its Effect on Long-Span Prestressed Concrete Box Girder Bridge," *Advances in Civil Engineering*, vol. 2020, no. 1, pp. 1-18, 2020. [CrossRef] [Google Scholar] [Publisher Link]

[2] Yumin Song et al., "Research on Temperature Distribution and Gradient Prediction of U-Shaped Girder Bridge under Solar Radiation Effect," *Applied Sciences*, vol. 14, no. 14, pp. 1-20, 2024. [CrossRef] [Google Scholar] [Publisher Link]

[3] Ali Hashemi, Javad Beheshti, and Mahdieh Mohammadi, "Physics-Based AI-Driven Surrogate Modeling for Structural Displacement Prediction in Mechanical Systems With Limited Sensor Data," *IEEE Access*, vol. 13, pp. 130585-130602, 2025. [CrossRef] [Google Scholar] [Publisher Link]

[4] Mahmoud Fadhel Idan, "The Role of Artificial Intelligence in Advancing Mechanical Engineering: Opportunities, Challenges, and Emerging Applications in Applied Mechanics," *Proceedings of the 8th International Conference on Applied Engineering (ICAE 2025)*, *Atlantis Press*, pp. 350-365, 2025. [CrossRef] [Google Scholar] [Publisher Link]

[5] Divyani Sen, Bharat Singh Deora, and Arun Vaishnav, "View of Explainable Deep Learning for Time Series Analysis: Integrating SHAP and LIME in LSTM-Based Models," *Journal of Information Systems Engineering and Management*, vol. 10, no. 16s, pp. 1-12, 2025. [CrossRef] [Google Scholar] [Publisher Link]

[6] Jiaxin Zhang, Congjie Wei, and Chenglin Wu, "Thermodynamic Consistent Neural Networks for Learning Material Interfacial Mechanics," *arXiv preprint*, pp. 1-7, 2020. [CrossRef] [Google Scholar] [Publisher Link]

[7] Zifei Xu et al., "Collaborative and Trustworthy Fault Diagnosis for Mechanical Systems Based on Probabilistic Neural Network with Decision-Level Information Fusion," *Journal of Industrial Information Integration*, vol. 46, pp. 1-20, 2025. [CrossRef] [Google Scholar] [Publisher Link]

[8] Yuqing Qiu et al., "Damage Identification for Bridges Using Machine Learning : Development and Application to KW51 Bridge," *Digital Engineering*, vol. 10, pp. 1-17, 2026. [CrossRef] [Google Scholar] [Publisher Link]

[9] Abdollah Malekjafarian et al., "A Machine Learning Approach to Bridge-Damage Detection Using Responses Measured on a Passing Vehicle," *Sensors*, vol. 19, no. 18, pp. 1-19, 2019. [CrossRef] [Google Scholar] [Publisher Link]

[10] Kang Yang et al., "Deep Learning-Based Bridge Damage Identification Approach Inspired by Internal Force Redistribution Effects," *Structural Health Monitoring*, vol. 23, no. 2, pp. 714-732, 2024. [CrossRef] [Google Scholar] [Publisher Link]

[11] Sardorbek Niyozov et al., "Temperature Effects Removal from Non-Stationary Bridge-Vehicle Interaction Signals for ML Damage Detection," *Sensors*, vol. 23, no. 11, pp. 1-26, 2023. [CrossRef] [Google Scholar] [Publisher Link]

[12] Taniya Kapoor et al., "Physics-Informed Neural Networks for Solving Forward and Inverse Problems in Complex Beam Systems," *IEEE Transactions on Neural Networks and Learning Systems*, vol. 35, no. 5, pp. 5981-5995, 2024. [CrossRef] [Google Scholar] [Publisher Link]

[13] NASA Prediction of Worldwide Energy Resources (POWER), Registry of Open Data on AWS. [Online]. Available: https://registry.opendata.aws/nasa-power/

[14] H. Elsom, and M. Pawley, "Extreme Value Statistics for Analysing Simulated Environmental Extremes," *Extremes*, vol. 28, pp. 47-73, 2025. [CrossRef] [Google Scholar] [Publisher Link]

[15] Lukas Brunner, and Aiko Voigt, "Pitfalls in Diagnosing Temperature Extremes," *Nature Communications*, vol. 15, pp. 1-9, 2024. [CrossRef] [Google Scholar] [Publisher Link]

[16] Suresh Kumar Padala et al., "Air Temperature Prediction Models for Pavement Design: A Gradient Boosting-Based Approach," *International Journal of Pavement Engineering*, vol. 25, no. 1, 2024. [CrossRef] [Google Scholar] [Publisher Link]

[17] ACI 209R-92, "*Prediction of Creep, Shrinkage, and Temperature Effects in Concrete Structures*," ACI Committee Report, pp. 1-47, 1997. [Google Scholar] [Publisher Link]

[18] Chengcheng Shen, Haifeng Zhao, and Jian Jiao, "A Multi-Subnets Physics-Informed Neural Network (Ms-PINN) Model for Transient Heat Transfer Analysis in Materials with Heterogeneous Microstructures," *Engineering with Computers*, vol. 41, pp. 3695-3717, 2025. [CrossRef] [Google Scholar] [Publisher Link]

[19] Ge Jin et al., "Fourier Warm Start for Physics-Informed Neural Networks," *Engineering Applications of Artificial Intelligence*, vol. 132, 2024. [CrossRef] [Google Scholar] [Publisher Link]

[20] Yanjia Wang et al., "Hybrid Physics-Informed Neural Network with Parametric Identification for Modeling Bridge Temperature Distribution," *Computer-Aided Civil and Infrastructure Engineering*, vol. 40, no. 22, pp. 3503-3524, 2025. [CrossRef] [Google Scholar] [Publisher Link]

[21] Rahul Suresh et al., "Revolutionizing Physics: A Comprehensive Survey of Machine Learning Applications," *Frontiers in Physics*, vol. 12, pp. 1-31, 2024. [CrossRef] [Google Scholar] [Publisher Link]

[22] Xi'an Li et al., "Physical Informed Neural Networks with Soft and Hard Boundary Constraints for Solving Advection-Diffusion Equations using Fourier Expansions," *Computers & Mathematics with Applications*, vol. 159, pp. 60-75, 2024. [CrossRef] [Google Scholar] [Publisher Link]

[23] Ziad Aldirany et al., "Operator Approximation of the Wave Equation based on Deep Learning of Green's Function," *Computers & Mathematics with Applications*, vol. 159, pp. 21-30, 2024. [CrossRef] [Google Scholar] [Publisher Link]
[24] Yiming Lu et al., "Enhanced Physics-Informed Neural Networks Using Adaptive Residual Weighting for Flow Simulations," *Proceedings of Global Power and Propulsion Society*, Shanghai, pp. 1-14, 2025. [CrossRef] [Google Scholar] [Publisher Link]
[25] Youqiong Liu et al., "Variable Separated Physics-Informed Neural Networks based on Adaptive Weighted Loss Functions for Blood Flow Model," *Computers & Mathematics with Applications*, vol. 153, pp. 108-122, 2024. [CrossRef] [Google Scholar] [Publisher Link]
[26] Yeonhwi Jeong et al., "Combined Analysis of Thermofluids and Electromagnetism Using Physics-Informed Neural Networks," *Engineering Applications of Artificial Intelligence*, vol. 133, 2024. [CrossRef] [Google Scholar] [Publisher Link]
[27] Xiaoli Wang et al., "Data-Driven Soliton Solutions and Parameters Discovery of the Coupled Nonlinear Wave Equations via a Deep Learning Method," *Chaos, Solitons & Fractals*, vol. 180, 2024. [CrossRef] [Google Scholar] [Publisher Link]
[28] Nirmal Patel, Aycin Aykutalp, and Pablo Laguna, "Novel Approach to Solving Schwarzschild Black Hole Perturbation Equations via Physics Informed Neural Networks," *General Relativity and Gravitation*, vol. 56, 2024. [CrossRef] [Google Scholar] [Publisher Link]
[29] Yushi Shan et al., "GNN-LSTM-based Full-Field Temperature Prediction of Bridges Using Sparse Sensor Data and Heat-Transfer Analysis," *Engineering Structures*, vol. 342, 2025. [CrossRef] [Google Scholar] [Publisher Link]
[30] Moez Krichen, and Alaeddine Mihoub, "Long Short-Term Memory Networks : A Comprehensive Survey," *AI*, pp. 1-21, 2025. [CrossRef] [Google Scholar] [Publisher Link]
[31] Federico Landi et al., "Working Memory Connections for LSTM," *Neural Networks*, vol. 144, pp. 334-341, 2021. [CrossRef] [Google Scholar] [Publisher Link]
[32] Ivan Malashin et al., "Applications of Long Short-Term Memory (LSTM) Networks in Polymeric Sciences: A Review," *Polymers*, vol. 16, no. 18, pp. 1-44, 2024. [CrossRef] [Google Scholar] [Publisher Link]
[33] S. Mariani et al., "Data-Driven Modeling of Long Temperature Time-Series to Capture the Thermal Behavior of Bridges for SHM Purposes," *Mechanical Systems and Signal Processing*, vol. 206, pp. 1-13, 2024. [CrossRef] [Google Scholar] [Publisher Link]
[34] Linren Zhou, Taojun Wang, and Yumeng Chen, "Bridge Temperature Prediction Method Based on Long Short-Term Memory Neural Networks and Shared Meteorological Data," *Advances in Structural Engineering*, vol. 27, no. 8, pp. 1349-1360, 2024. [CrossRef] [Google Scholar] [Publisher Link]
[35] Aiping Guo et al., "Data Mining Algorithms for Bridge Health Monitoring: Kohonen Clustering and LSTM Prediction Approaches," *The Journal of Supercomputing*, vol. 76, pp. 932-947, 2019. [CrossRef] [Google Scholar] [Publisher Link]
[36] Yuching Wu et al., "Finite Element Analysis of Perforated Prestressed Concrete Frame Enhanced by Artificial Neural Networks," *Buildings*, vol. 14, no. 10, pp. 1-18, 2024. [CrossRef] [Google Scholar] [Publisher Link]
[37] Shahin Alipour Bonab, Wenjuan Song, and Mohammad Yazdani-Asrami, "Physics-Informed Neural Network Model for Transient Thermal Analysis of Superconductors," *Superconductor Science and Technology*, vol. 38, pp. 1-11, 2025. [CrossRef] [Google Scholar] [Publisher Link]
[38] Eurocode 1: Actions on structures - Part 1-5: General actions - Thermal Actions, European Commitee for Standardization, 2003. [Online]. Available: https://www.phd.eng.br/wp-content/uploads/2015/12/en.1991.1.5.2003.pdf
[39] Bridge Manual SP/M/022, no. SP/M/022, NZ Transport Agency, 2022. [Online]. Available: https://www.nzta.govt.nz/resources/bridge-manual
[40] Sallal R. Abid, "Three-Dimensional Finite Element Temperature Gradient Analysis in Concrete Bridge Girders Subjected to Environmental Thermal Loads," *Cogent Engineering*, vol. 5, no. 1, pp. 1-15, 2018. [CrossRef] [Google Scholar] [Publisher Link]
[41] M. J. Nigel Priestley, "Design of Concrete Bridges for Temperature Gradients," *American Concrete Institute Journal*, pp. 209-217, 1978. [CrossRef] [Google Scholar] [Publisher Link]
[42] Ethiopia Road Administration, Bridge Design Manual - Part 1, 2013. [Online]. Available: https://bms.era.gov.et:8087/media/bridge/Combolcha/Dichoto/Mille%20-%20Semera/A1-7-009/R52.pdf
[43] Shijun Huang et al., "Multi-Field Numerical Model and LSTM-based Neural Networks for Thermal Field Predictions of Concrete-Filled Steel Tubes," *Frontiers in Materials*, vol. 12, pp. 1-13, 2025. [CrossRef] [Google Scholar] [Publisher Link]
[44] Vishnu Sharma, and A.K. Dwivedi, "Effect of Temperature Stresses in Composite Girder Bridges," *International Journal of Research and Scientific Innovation*, vol. 5, no. 8, pp. 97-101, 2018. [Google Scholar] [Publisher Link]
[45] Da Wang et al., "Numerical Investigation of Temperature Gradient-Induced Thermal Stress for Steel-Concrete Composite Bridge Deck in Suspension Bridges," *Journal of Central South University*, vol. 25, pp. 185-195, 2018. [CrossRef] [Google Scholar] [Publisher Link]
[46] Jiahao Song et al., "VW-PINNs: A Volume Weighting Method for PDE Residuals in Physics-Informed Neural Networks," *Acta Mechanica Sinica*, vol. 41, 2025. [CrossRef] [Google Scholar] [Publisher Link]
[47] Xiaoting Yang et al., "Longitudinal Displacement Reconstruction Method of Suspension Bridge End Considering Multi-Type Data Under Deep Learning Framework," *Buildings*, vol. 15, no. 15, pp. 1-19, 2025. [CrossRef] [Google Scholar] [Publisher Link]
[48] Shaolun He et al., "Effect of Temperature Gradients on the Microstructural Characteristics and Mechanical Properties of Concrete," *Cement and Concrete Research*, vol. 184, 2024. [CrossRef] [Google Scholar] [Publisher Link]

[49] R. Sharmaa, and Y.B. Guo, "Thermal-Mechanical Physics Informed Deep Learning for Fast Prediction of Thermal Stress Evolution in Laser Metal Deposition," *arXiv preprint*, pp. 1-18, 2024. [CrossRef] [Google Scholar] [Publisher Link]

[50] Yushi Shan et al., "Temperature Behavior of Cable-Stayed Bridges. Part I — Global 3D Temperature Distribution by Integrating Heat-Transfer Analysis and Field Monitoring Data," *Advances in Structural Engineering*, vol. 26, no. 9, pp. 1579-1599, 2023. [CrossRef] [Google Scholar] [Publisher Link]

[51] Sallal R. Abid, Nildem Tayşi, and Mustafa Özakça, "Experimental Analysis of Temperature Gradients in Concrete Box-Girders," *Construction and Building Materials*, vol. 106, pp. 523-532, 2016. [CrossRef] [Google Scholar] [Publisher Link]

[52] Yousong Peng, and Shizhong Qiang, "Analytical Solution to Temperature Variations in Highway Concrete Bridges Due To Solar Radiation," *International Conference on Transportation Engineering*, pp. 1536-1541, 2007. [CrossRef] [Google Scholar] [Publisher Link]

[53] R. Mahto, "Thermal Stress Analysis in Pre-Stressed Concrete Bridges using COMSOL Multiphysics," *International Journal of Surveying and Structural Engineering*, vol. 6, no. 1, pp. 27-32, 2025. [CrossRef] [Publisher Link]

[54] Federal Highway Administration, *Chapter 5: Assessment of Bridge Fatigue and Investigation into Bridge Deck Wear*," Comprehensive Truck Size and Weight Limits Study: Bridge Structure. Comparative Analysis Technical Report, U.S. Department of Transportation. 2025. [Publisher Link]